This article has been accepted for publication in IEEE Transactions on Components, Packaging and Manufacturing Technology. This is the author's version which has not been fully edited and content may change prior to final publication. Citation information: DOI 10.1109/TCPMT.2024.3464243

A Wideband Transition from Coaxial Line to Substrate Integrated Waveguide

Anil Kumar Nayak, *Graduate Student Member, IEEE*, Igor M Filanovsky, *Life Senior Member, IEEE*, Kambiz Moez, *Senior Member, IEEE*, Amalendu Patnaik, *Senior Member, IEEE*

***Abstract*—This paper presents a novel broadband transition from coaxial line to substrate-integrated waveguide (SIW). The SIW wall includes three rows of metallic vias, where the vias of smaller diameter are squeezed between vias of larger diameter. This modification results in a corrugated via-wall SIW (CVWSIW) providing lower loss. Three versions of stubs (rectangular, semicircular, and triangular) are designed around the coaxial line launch on the top metal plane of the SIW. All transition versions are fabricated and tested, and the measurement results are in a good agreement with simulations. The measured more than 14 dB return loss (RL), fractional bandwidth (FBW) of 75, 79.4, and 44.6% (10 dB FBW: 97.14, 90.5, and 78.26%) in these versions for the 9-26 GHz frequency range were obtained, respectively. The insertion loss (IL) is less than 0.63, 0.91, and 0.68 dB; the total loss is below 20, 30, and 25% for these versions for the same frequency band, respectively.**

***Index Terms*—Corrugated via-wall substrate integrated waveguide (CVWSIW), Coaxial line-to-CVWSIW transition, Ku-band, Broadband transition.**

I. Introduction

MICROWAVE transmission lines (TLs), coaxial lines, and waveguides are widely used to connect various devices operating at microwave frequencies such as antennas, filters, amplifiers etc. As a microwave system may include several types of TLs, coaxial lines and waveguides, the transitions from one type of carrier to another are needed. These transitions must exhibit low insertion and leakage losses and high return loss while they must be compact and have reduced fabrication cost. For example, the conventional rectangular waveguides (CRWs) have high-power handling capabilities and low losses at mm-wave frequencies [1], [2], but they are heavy, expensive, and require transitions for their operation together with other TLs. The planar microstrip technology offers small form factor, low profile, lightweight, and inexpensive fabrication [3], [4]. However, at millimeter-wave (mm-wave) frequencies, the planar microstrip devices have significant losses, high radiation leakage, undesired coupling between adjacent elements, and limited power handling capabilities. To improve these parameters, a new concept of substrate integrated waveguide (SIW) was introduced in 1998 [4] and implemented in planar technology in 2001 [5]. In the mm-wave and THz frequency range, the SIWs often exhibit better RF performance than the planar microstrip lines owing to their low insertion losses, higher quality factor, and wider bandwidth. They are easily integrated with other planar components [6]. Yet, one must accept, they still have lower power handling capabilities and lower quality factors than CRWs.

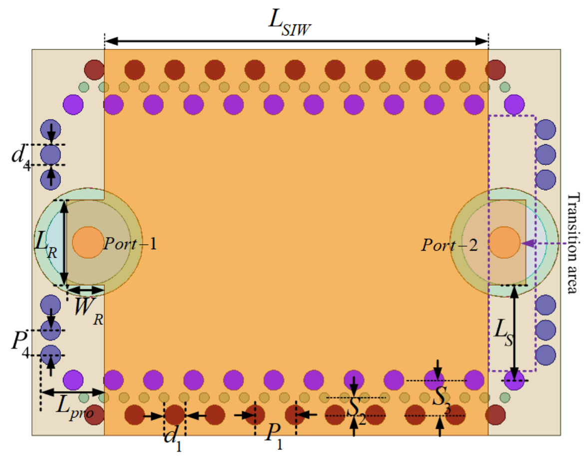

(a)

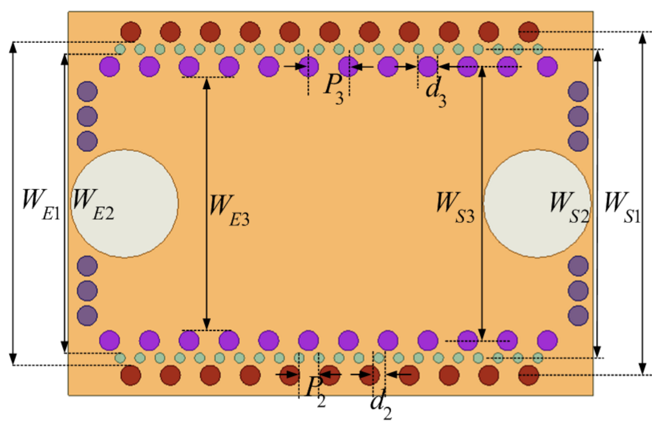

(b)

Fig. 1. The proposed transition (the version with rectangular stubs shown only): (a) Top view, (b) Bottom view (this view is common for all shapes of stubs).

Despite the advances of SIWs, the development of a low-loss interface between the coaxial line and SIW remains a challenging problem [7]–[12]. In addition, the development of transition between the coaxial line and SIW is usually [13]–[24] (and here as well), simultaneously improving the

Manuscript received August 8, 2022; Anil Kumar Nayak and Amalendu Patnaik are with the Department of Electronics and Communication Engineering, Indian Institute of Technology, Roorkee, Uttarakhand, 247667, India.
(E-mail: anayak@ec.iitr.ac.in; amalendu.patnaik@ece.iitr.ac.in).
Anil Kumar Nayak, Igor M Filanovsky, and Kambiz Moez are with the Department of Electrical and Computer Engineering, University of Alberta, Alberta, Canada
(E-mail: aknayak@ualberta.ca; ifilanov@ualberta.ca; kambiz@ualberta.ca)

qualities of SIW. The design and analysis of corrugated shapes in microstrip applications, especially for antennas, started long ago [25]–[27]. Many benefits, such as a reduction in the overall losses, decrease in the spillover, increase in the aperture efficiency, reduction in the cross-polarization, and improvement in the antenna directivity, were found. Gradually, these concepts were applied to the design of waveguide walls [28]–[32], resulting in the corrugated via-wall SIW (CVWSIW). The advantages of CVWSIW over SIW are lower loss, enhanced bandwidth, and improved signal integrity in exchange for a negligible increase in size and fabrication cost. The corrugated techniques also offer a more stable signal transmission, making them suitable for harsh environments such as aerospace, automotive, and industrial applications. The coaxial feeding technique is advantageous in specific issues, e.g., low spurious radiation, low cost, good bandwidth, etc. However, matching the SIW to the coaxial port is challenging, especially in the case of a thin substrate.

In the present work, a broadband transition (in three versions) from coaxial line to SIW is proposed (Fig. 1). To decrease the loss, the SIW corrugated wall is improved using three rows of vias. The open stubs (metallic patches) of rectangular, semi-circular, or triangular shapes are used at the top metallic plane around the feed. These forms are investigated to evaluate which one provides better impedance matching and broader bandwidth with the most compact size of the transition area. Additionally, we have used six metallic vias near the stubs at both Port 1 and 2, helping to further reduce the transition area Three versions corresponding to these stubs (Transition I, II, and III) were fabricated and tested.

The paper is structured as follows. The layout and design of the transitions are presented in Section II. Section III depicts the transition prototypes, the measurement setup, and the results. The comparison table is also given. Finally, the conclusions of the work are provided in Section IV.

II. Design and Analysis of the Broadband Transitions

The top and bottom views of the proposed transition are shown in Fig. 1. The traditional SIW is designed with one row of vias [10], [11]. But the simulation results of the initially proposed one-row SIW indicated unsatisfactory transmission and reflection characteristics. In particular, the simulation indicated that the return loss for the Ku-band was limited to 10 dB. CVWSIWs with four different structures (see Fig. 2(a)) of via walls are simulated without the transition in order to compare the performance of all four structures, eliminating the effect of the impedance mismatch on the results. The simulated $|S_{11}|$ and $|S_{21}|$ of these four structures are plotted in Fig. 2(b). As illustrated in Fig. 2(c), the insertion loss of the proposed 3-row structure is significantly lower than all three other wall structures In addition, the proposed wall structure was established in four steps (shown in Fig. 2(a)), resulting in the described wall. The three rows create more "dense" electrical walls reducing the radiation leakage loss, which is the largest part of the overall loss or total loss (TL) given by $1-|S_{11}|^2-|S_{21}|^2$.

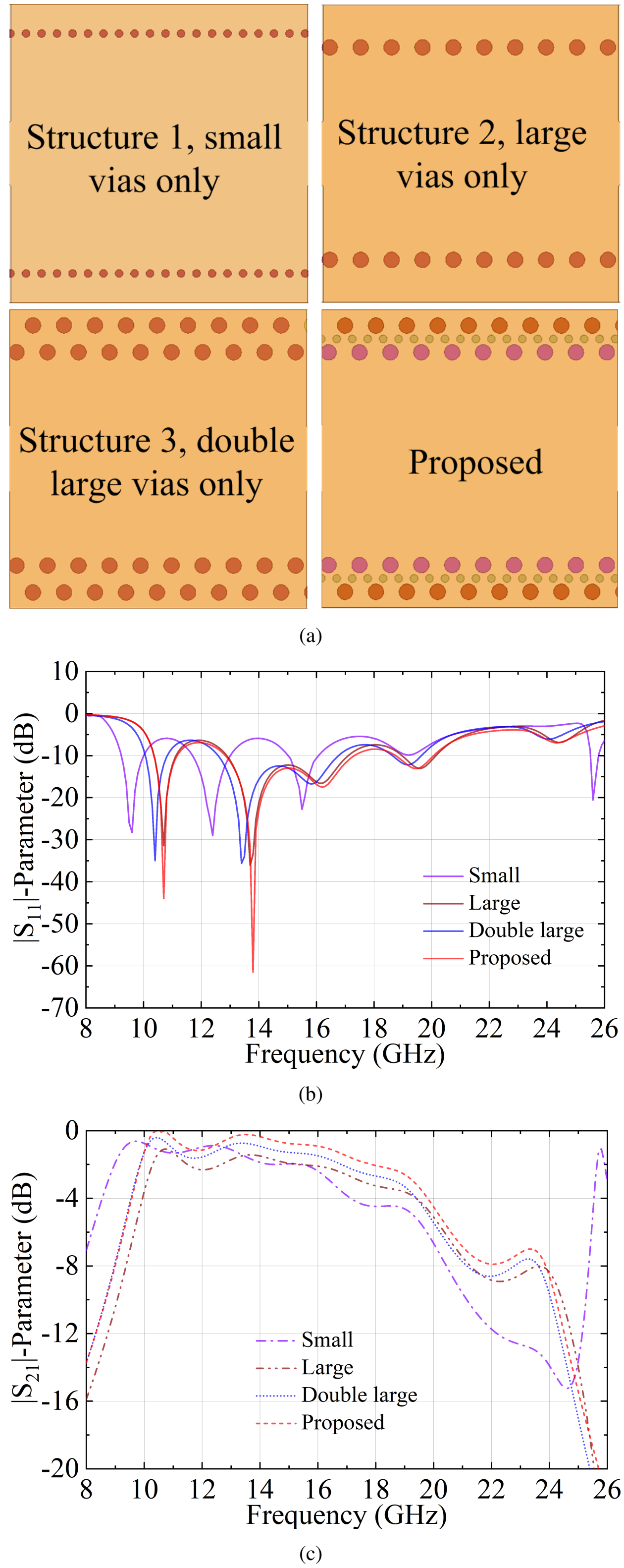

Fig. 2. (a) Different wall structures of CVWSIW without transitions, simulated (b) $|S_{11}|$ (c) $|S_{21}|$-parameters.

We have simulated the transitions with different wall structures to compare the performance of the walls. Fig. 2(a) shows the simulated wall designs: (1) single thin via wall, 2) single large via wall, 3) double large via wall, and 4) proposed

This article has been accepted for publication in IEEE Transactions on Components, Packaging and Manufacturing Technology. This is the author's version which has not been fully edited content may change prior to final publication. Citation information: DOI 10.1109/TCPMT.2024.3464243

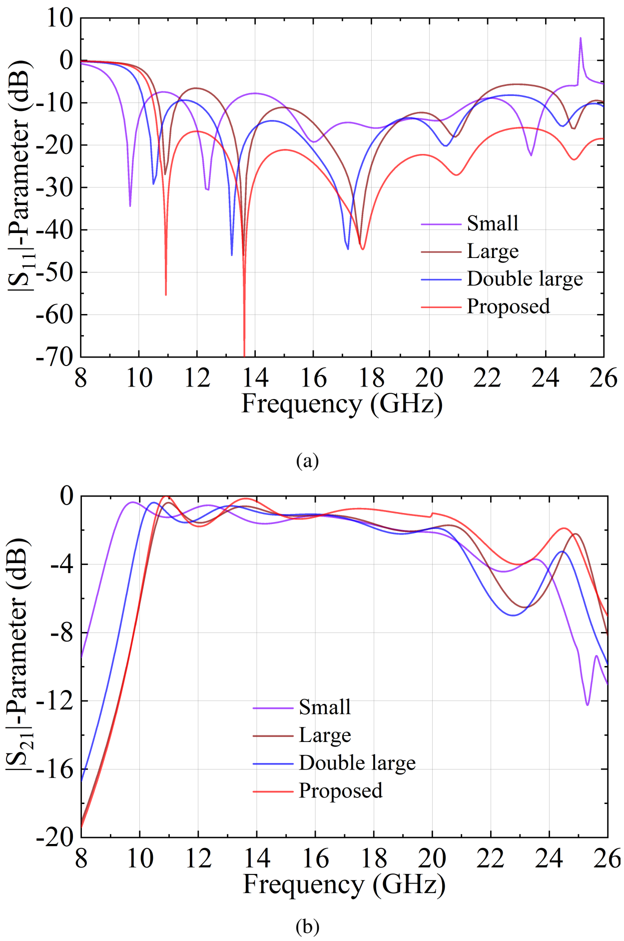

Fig. 3. Simulated S-parameters of the different structures of wall modification with transition (see Fig. 2 (a)): (a) $|S_{11}|$ (b) $|S_{21}|$.

three-row wall. Fig. 3 (a) and (b) shows the S-parameters for the transition with circular stubs (the results for other stubs are similar). One can see that the proposed three-row wall produces a superior RF performance with respect to other wall structures. It can be observed from these results that the proposed construction of the SIW wall increases the operation bandwidth of the transition while lowering its insertion and input/output return losses.

The dimensions of elements (vias, their diameters, and the distance between them) are chosen considering the dominant or fundamental mode (TE_{10}) of the rectangular waveguide with a cutoff frequency f_c in 8 to 26 GHz range. The diameter of vias d_i, pitch distance P_i, and equivalent width W_{Ei} should be connected by the following relationships [5], [33]:

$$f_c = \frac{c}{2W_{Ei}\sqrt{\varepsilon_r}}; \lambda_g = \frac{\lambda_0}{\sqrt{\varepsilon_r}}; d_i \leq \frac{\lambda_g}{5}; P_i \leq 2d_i \quad (1)$$

$$W_{Ei} = W_{Si} - 1.08\frac{d_i^2}{P_i} + 0.1\frac{d_i^2}{W_{Si}}, i = 1, 2, 3 \quad (2)$$

Here λ_g is the guided wavelength at the center frequency, λ_0 is the wavelength in the free space or air, and ε_r is the relative dielectric constant of the substrate, c is the speed of light. These relationships should be satisfied for each component of

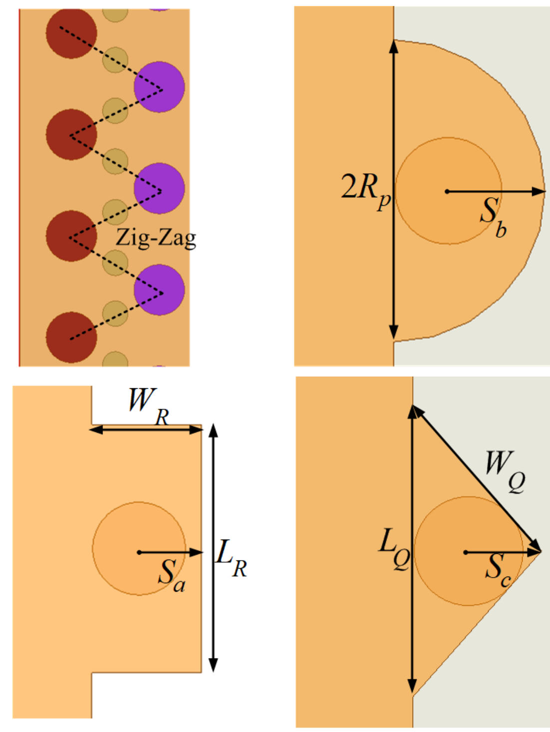

Fig. 4. Zig-zag vias pattern and stubs of different shapes in the coaxial line attachment area.

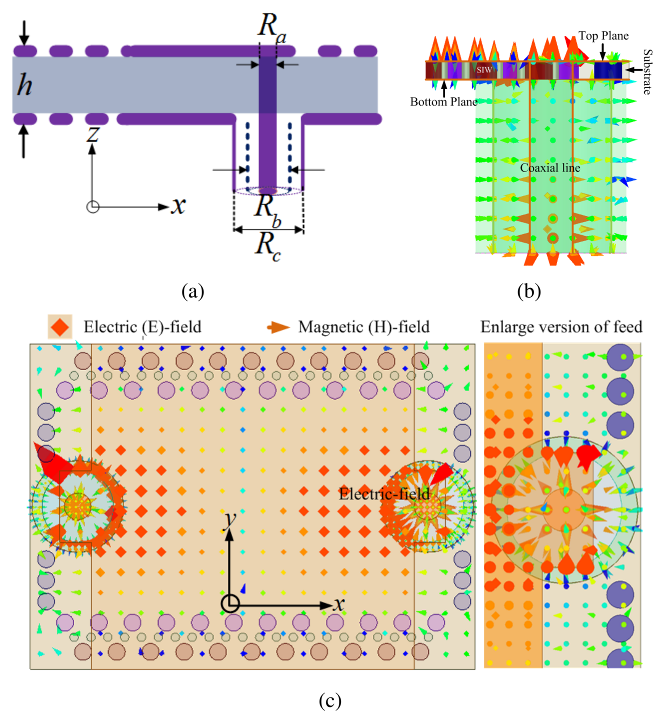

Fig. 5. The proposed transition: (a) Coaxial line (R_a=0.6, R_b=1.6, and R_c=4.35 all in mm), (b) $\vec{E}$ on the xz-plane, (c) Field distribution ($\vec{E}$ and $\vec{H}$) in the middle of the SIW or xy-plane inside the substrate at 17.5 GHz.

the corrugated wall. These "dense" walls help as well to obtain a wider bandwidth and better mode conversion (see above). The wall of CWSIW shows the zig-zag pattern (Fig. 4, top left corner). The distance between center to center of each row of vias is S_2 and the distance between the first and third row of vias is S_3 (see Fig. 1 (a)). These S_2 and S_3 are playing a significant role in reducing loss and improving the impedance bandwidth [34], [35]. The values of S_2 and S_3 chosen after extensive simulations are 0.695 and 1.39 mm, respectively. In addition, the value of $S_2/d_2 = S_3/d_1 = S_3/d_3$ are fixed at 1.73. Similarly, the values of $S_3/P_1 = S_3/P_3$ and S_2/P_2 are equal to 0.86 and 0.46. respectively. The final dimensions of transition are: $d_1 = 0.8$, $P_1 = 1.6$, $d_2 = 0.4$, $P_2 = 1.5$, $d_3 = 0.8$, $P_3 = 1.6$, $d_4 = 0.7$, $P_4 = 1.1$, $L_{SIW} = 15.3$, $L_S = 3.8$, $W_{S1} = 13.78$, $W_{S2} = 12.39$, $W_{S3} = 11.0$ $W_{E1} = 13.35$, $W_{E2} = 12.28$, $W_{E3} = 10.57$; unit: millimeters. The formulas (1) and (2) should be approximately valid for any row of vias.

The coaxial line is connected vertically to the open-circuited SIW, as shown in Fig. 5(a). The inner conductor having diameter R_a is connected to the top cladding conducting metal plane. The outer shell of diameter R_c is connected to the bottom metal plane. In addition, a circular hole of diameter R_b is etched from the bottom cladding conductor, creating a plane of excitation to utilize the perfect magnetic conductor (PMC). Also, it behaves as an open circuit or artificial magnetic wall due to a higher width-to-height ratio [36]. The middle insulator is the Teflon of diameter R_b, which is touching the bottom of the substrate plane. The electric field ($\overrightarrow{E}$) distribution of the coaxial line on the xz-plane is shown in Fig. 5(b). It can be observed the $\overrightarrow{E}$ passes through the central conductor or axis of the outer conductor. Consequently, the transverse electromagnetic (TEM)-mode is transformed into the transverse electric (TE)-mode. The $\overrightarrow{E}$ distributions center of SIW (top metallic plane) is illustrated in Fig. 5(c). It can be concluded that the dominant mode (TE_{10}) is excited inside the SIW. In general, one is trying to create the best conditions for probe-fed excitation of the rectangular waveguide [1], and this explains using the additional metal vias at the perpendicular outer edges of the transition. This second modification of [10], [11] is "moving" (in an electromagnetic sense) the feeding wire into SIW and is helping to achieve a better impedance matching of the transition and, together with the modified SIW wall to reduce the lateral leakage loss.

The next aim of this work is to optimize the transition area and make the structure more compact while preserving the bandwidth. Considering that the area around the line conductor plays an active role in TEM to TE mode transforming, three different shapes (rectangular, semi-circular, and triangular) are implemented on the top metal plane (Fig. 4). The exact dimensions of these shapes are evaluated using parametric analysis. For example, for the semicircular patch (Transition II) the radius R_p is varied from 1.6 to 2.0 mm with a step size of 0.1 mm. For this variation, the return loss shows a significant variation. It was observed that, the return loss is best at R_p=1.8 mm. The -10 and -15 dB of $|S_{11}|$ the impedance BW of 15.5 and 11.5 GHz were achieved between 10 and 26 GHz frequency range with R_p=1.8 mm. The minimum and maximum $|S_{21}|$ of -0.16 and -2.08 dB for these bands were also obtained. Thus,R_p was finalized and chosen to be 1.8 mm. The S-parameters for this value of R_p are given in the next part. Similarly, the dimensions of the other two shapes (rectangular: Transition I and triangular: Transition III) were

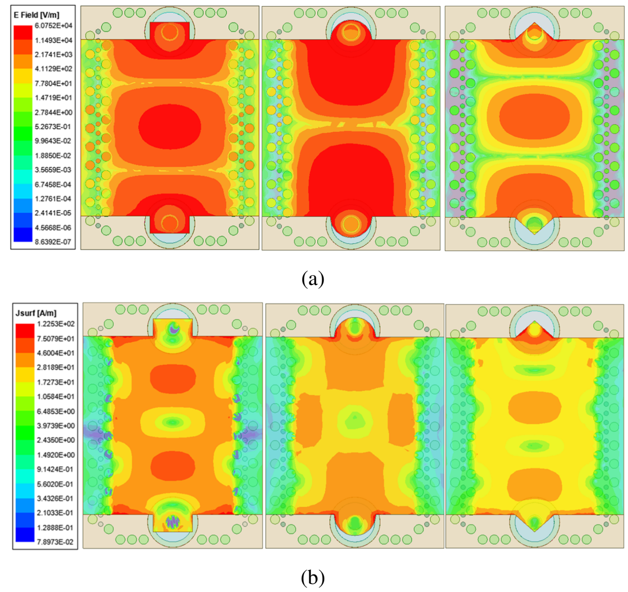

Fig. 6. The electric field (a) and the surface current (b) distributions at 17.5 GHz.

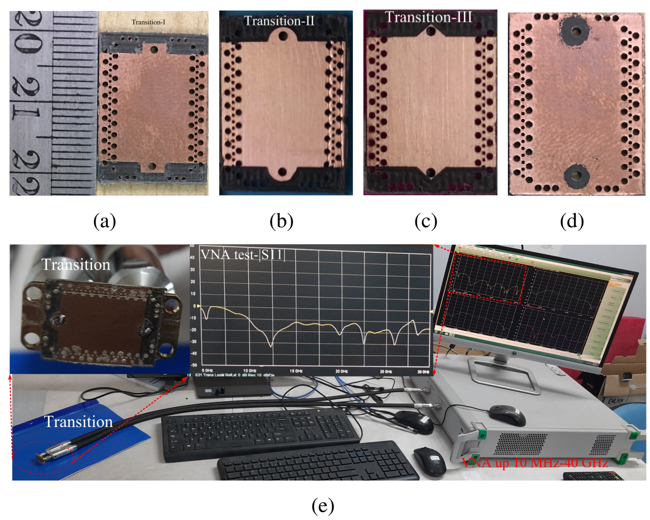

Fig. 7. The fabricated prototypes (top views and bottom view) and measurement setup:(a) Transition I, (b) Transition II, (c) Transition III,(d) Bottom view of all transition versions, and (e) The back-to-back transitions with VNA.

evaluated by using parametric analysis. The longest length of the rectangular shape is L_R, whereas the base of a triangular stub is L_Q. So, L_R and L_Q are varied from 3.2 to 3.6 mm with a step size of 0.1 mm. The best-simulated results for $|S_{11}|$ and $|S_{21}|$ are found for $L_R = L_Q$ =3.4 mm (they are also given in the next section). In addition, the values of S_a, S_b, and S_c (see Fig. 4) are fixed at 0.85, 1.15, and 0.85 mm respectively, to avoid the surface wave losses. In addition, we have simulated different wall structures of the transitions to compare the performance of the walls with different wall densities. Fig. 3 (a) shows the simulation results for 1) single small via wall, 2) single large via wall, 3) double large via wall, and 4) proposed three-row wall for the transition with rectangular stubs. One can see that the proposed three-row wall structure produces a superior RF performance to all three

Table I
COMPETITIVE BROADBAND TRANSITIONS BETWEEN THE COAXIAL LINE TO SIW

Reference	Frequency (GHz)	10 dB FBW (%)	IL (dB)	Size (λ_g^2)	Total loss (%)	Design complexity	FOM
[22]	9.3-15.2	48.1/44.9^b	1±0.1	1.187	NR	Simple	36.53/34.10^b
[23]	18-26	36.3	0.9-1.3	NR	NR	Moderate	DI
[24]	18-32	20/14^b	0.6/0.7	NR	NR	Moderate	DI
[7]	55-65	16.7/14.7^b	≈0.65-1.9	2.84	NR	Moderate	5.1/4.25^b
[15]	4.24-8.04	63.34	0.16-1.08	NR	17-25	Simple	DI
[18]	71-86	28.57/22^b	≤0.5	0.315 (0.0201*)	NR	Moderate	85.64/65.93^b
[9]	50-70	11.3	≤0.8	NR	<8	Moderate	DI
[8]	59-67	12.69	0.6 (minimum)	0.384	NR	Moderate	30.84
[11]	8-12	50/48.5^b	≤0.75	0.08	<15	Simple	573.4/556.2^b
[20]	8-12	37.83/30^b	≈1^a	0.6	NR	Simple	56.19/44.56^b
[10]	8-12	35.9/30^b	≤ 1.2	0.3	NR	Simple	104.3/87.1^b
[12]	8-12	46.15/43.4^b	≤1	0.156	NR	Simple	269.9/242.4^b
[21]	12-18	40	≤0.83	NR	NR	Moderate	DI
This work	**9-26/10-22^c (Transition I)** **9.8-26/9.5-22^c (Transition II)** **9.8-22.4/12.9-20.3^c (Transition III)**	**97.1/75^c** **90.5/79.36^c** **78.6/44.57^c**	≤0.63 ≤.0.91 ≤0.68	**0.035** **0.035** **0.0175**	**<20** **<30** **<25**	**Simple**	**2581/1992.9^c** **2328.5/2041^c** **4135/2355^c**

(∗): in terms of λ_0^2; **NR**: Not reported; ^{a}: 5% of 20 dB; ^{b}: 15 dB FBW; ^{c}: >14 dB FBW; DI: Data insufficient

other wall structures. It can be observed from these results that the proposed construction of SIW wall increases the operation bandwidth of the transition while lowering its insertion and input/output return losses. The electric field and the surface current distributions are calculated at 17.5 GHz (mid-band) and are shown in Fig. 6.

III. EXPERIMENTAL VALIDATION AND DISCUSSION

Fig. 7 shows the prototypes of back-to-back versions of the proposed transition and the experimental setup for the measurements with a vector network analyzer (VNA). In Fig. 7(a)-(c), top views of three fabricated versions with the different stubs (rectangular, semi-circular, and triangular) are given. The bottom plane (Fig. 7(d)) is kept identical for all three versions. The transition is designed on a single layer Rogers RT/Duroid 5880 (tm) substrate with a dissipation factor $(\tan(\delta))$ = 0.0009, ε_r = 2.2, and h = 0.71 mm. All the simulations were carried out using Ansys HFSS ver. 2020R2.The electronics calibration (Ecal) method was used for measurements, and the set view is shown in Fig. 7(e).

The simulated and measured results of Transition I are illustrated in Fig. 8(a)). For -10 dB value of $|S_{11}|$, the bandwidths are 15.72 (simulated) and 17 GHz (measured). For the value of -14 dB the bandwidth of 15.58 (simulated) and 16.4 GHz (measured) are achieved. The minimum and maximum values of insertion losses obtained by simulations are 0.14 and 1.51 dB, respectively, whereas the experimental values are 0.16 and 1.11 dB in the frequency range of 10-22 GHz. The simulated and measured insertion loss are more than 1.51 and 1.11 dB above 22 GHz value. Further, the sources of loss from the fabricated transition are investigated. The overall loss $(1-|S_{11}|^2-|S_{21}|^2)$ is dependent on the $|S_{11}|$ and $|S_{21}|$. The simulated and measured values of the total loss are shown in Fig. 8 (b). The measured total loss is within 30- percent (<30%) over the 8-22.8 GHz. Also, the total loss is below 20% at the frequency 9.8-18.9 GHz range.

The Transition II (semi-circular stub) and Transition III (triangular stub) were also fabricated (Fig. 7 (b) and (c)). S-parameters for these versions are illustrated in Fig. 9 and 10, respectively. The simulated results of -10 and -15 dB value bandwidth of 15.48 and 15.39 GHz are obtained for Transition II. The measured values -10 and -14 dB absolute bandwidth of 16.2 and 15.75 GHz are achieved. The minimum simulated and measured insertion loss values of 0.16 and 0.14 dB (maximum values are 1.96 and 1.69 dB) are realized. It can be observed from Fig. 9 (b) that the insertion loss is slightly higher at frequencies larger than 22 GHz. It may be because of the manual filling of copper paste into vias. For Transition III (triangular stub), the measured values of -10 and -15 dB value bandwidth of 12.6 and 7.4 GHz (simulated: 15.7 and 9 GHz) are found, as depicted in Fig. 10. The minimum and maximum measured insertion loss of 0.16 and 1.21 dB (simulated: 0.12 and 1.49 dB) are obtained over the frequency range of 10-22 GHz. The measured total loss is below 30% (10-21 GHz) for the Transition II and less than 28% (9.6-22.8 GHz) for Transition III as shown in Fig. 9(b) and 10 (b), respectively. The simulated loss is also found less than 30% for both Transition II and III.

In addition, we investigated the overall loss (or total loss $=1-|S_{11}|^2-|S_{21}|^2$) considering it as a combination of leakage loss, metallic or copper loss and dielectric loss. This was done in three structures.

1) Assuming the top cladding conductor and bottom cladding conductor ideal by defining them as perfect

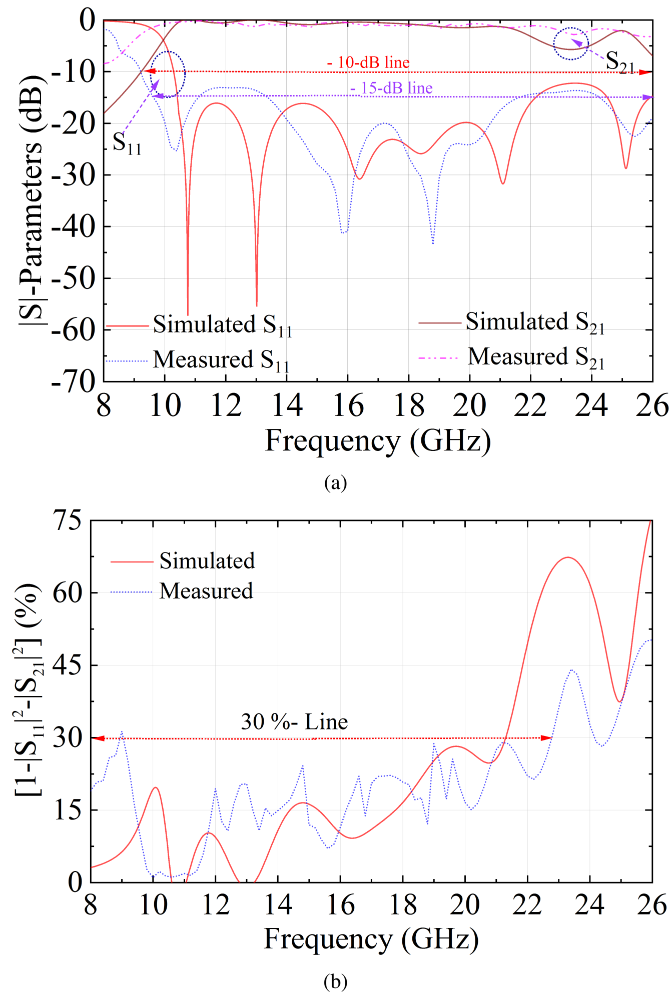

Fig. 8. Simulated and measured results of Transition I (rectangular stub): (a) $|S_{11}|$ and $|S_{21}|$ (b) Total loss.

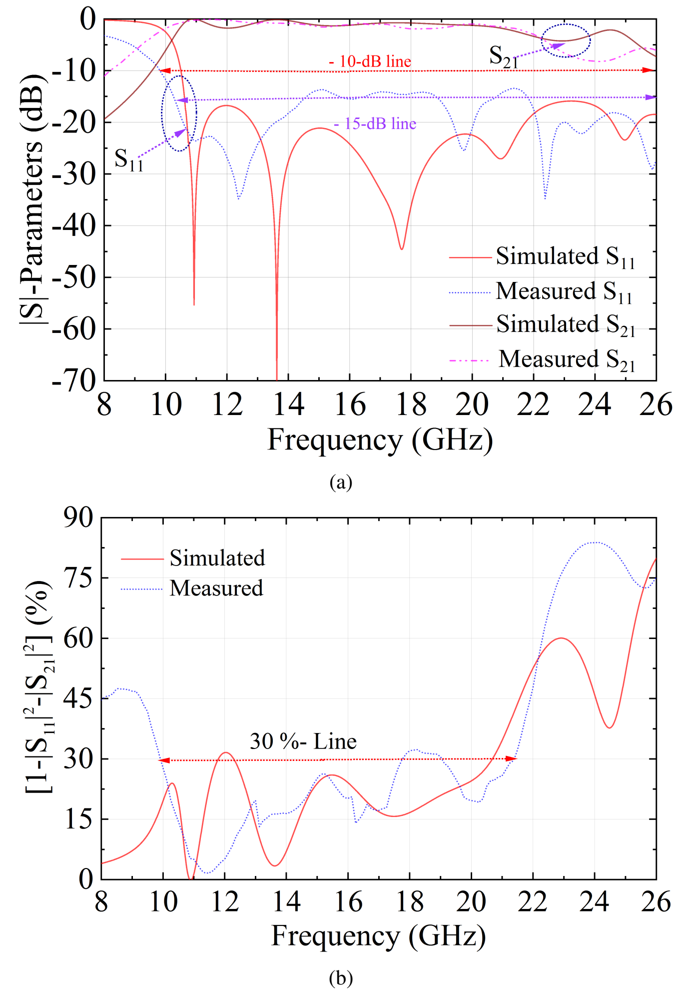

Fig. 9. Simulated and measured results of Transition II (semi-circular stub): (a) $|S_{11}|$ and $|S_{21}|$ (b) Total loss.

electric conductors (PEC) and the dielectric material as lossless, setting its loss tangent ($\frac{\sigma}{\omega\varepsilon} = 0$) equal to zero, we calculated the total loss. The simulated total loss, in this case, is caused only by the wall leakage. This was done for all walls as shown in Fig. 2(a). In this way, we confirmed once more that the proposed wall provides the lowest leakage loss (an example for the case with semicircular pads is shown in Fig. 11)). Structure 1 has almost the same leakage loss as Structure 2 because both structures use single rows of vias. After 20 GHz, it can be observed that the total leakage loss in Structure 2 is less than that in Structure 1. However, Structure 3 reduces this leakage loss by approximately 11 and 5% compared to Structure 1 and 2, respectively. At this Structure, the minimum and maximum leakage losses of the proposed transition are reduced by 7 and 25%, respectively, compared with Structure 1. Similarly, for the final Structure, the minimum and maximum leakage losses are less by 5 and 15%, respectively, compared to the previous structure. Finally, between Structure 3 and the proposed transition, the minimum and maximum leakage losses decrease by 4 and 14%, respectively (see Fig. 11).

2) Keeping the conductor as PEC, one assumes the dielectric with losses ($\tan\delta = 0.0009$). The simulated total loss, in this case, is the sum of wall leakage loss and dielectric loss. If necessary, the dielectric losses can be obtained by subtracting from this loss the leakage loss (calculated in Step 1).
3) We bring all losses into our simulation by assuming a finite conductivity for the metal layers (Cu) and loss tangent ($\tan\delta = 0.0009$) for the dielectric layer. The simulated total loss in this case is the sum of wall leakage loss, dielectric loss, and metal loss. The metal loss can be calculated by deducting the total loss calculated in Step 2 from this loss.

This sequence of simulations allows one to evaluate the contribution of each source of the losses. The result is shown in Fig. 12. One can see that the main contribution (first step, blue line) is provided by the leakage loss, the dielectric loss is indeed, adds a small contribution (green line), and the copper loss adds an irregular but sizable addition to the total loss (red line).

The length of SIW (L_{SIW}) is 15.3 mm. The minimum and maximum measured IL, including the loss of 6.15 mm

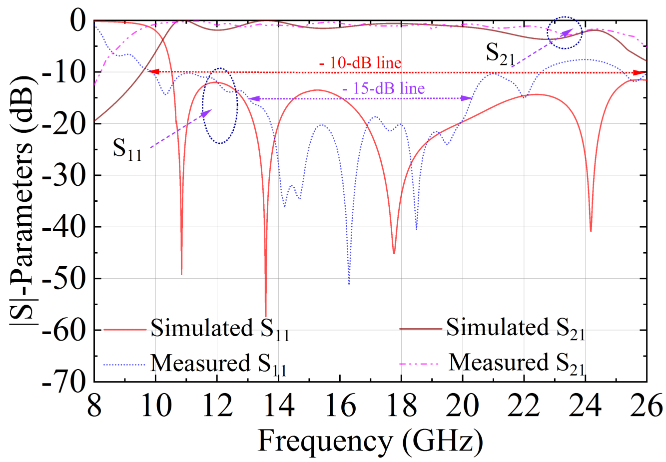

(a)

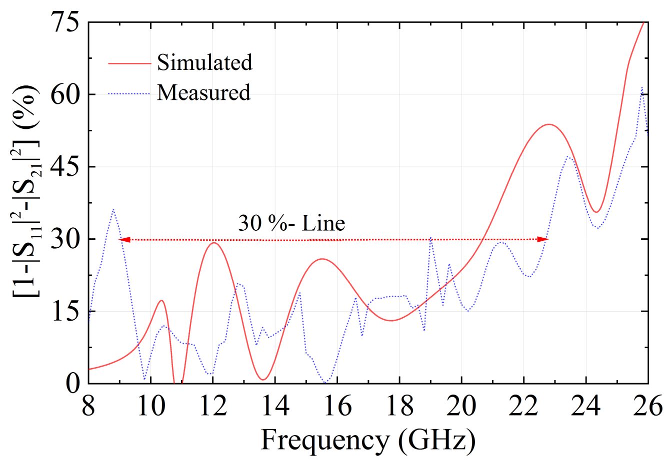

(b)

Fig. 10. Simulated and measured results of Transition III (triangular stub): (a) $|S_{11}|$ and $|S_{21}|$ (b) Total loss.

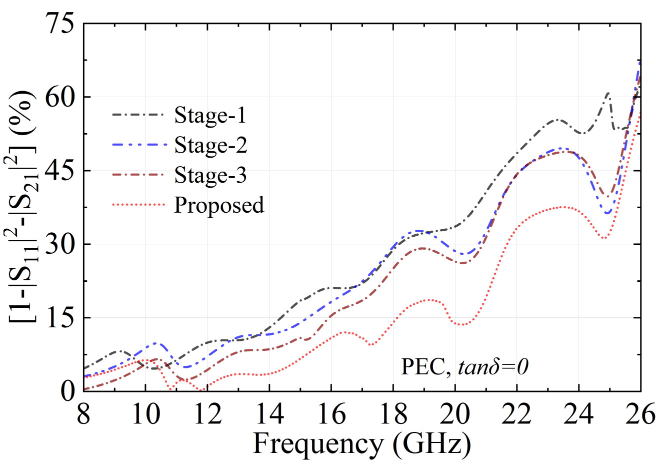

Fig. 11. Leakage losses for different walls with perfect electric conductor (PEC) and $\tan\delta = 0$ (semi-circular stub: see Fig. 3 (a)).

50- Ohm feeding lines obtained over the entire band, are of 0.37 and 0.83 dB, respectivelyfor probes. It infers that the minimum and maximum ILs are about 0.0073 dB/mm and 0.056 dB/mm in the entire band, respectively. For Transitions I, II, and III, the lengths of transitions are the same. The

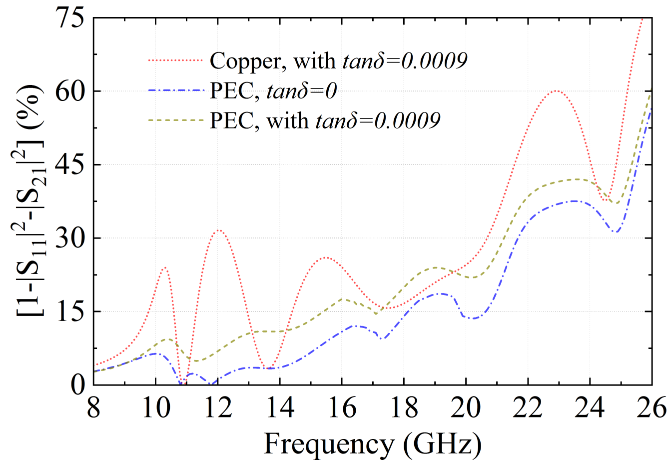

Fig. 12. Components of total transition losses (semi-circular stub).

insertion loss of 0.029, 0.042, and 0.031 dB/mm for three transitions (Transition I, II, and III) are obtained, respectively. The simulation results are confirmed with the measured results.

Table I summarizes the performance of the proposed design and gives a comparison with the previously reported works. The proposed design operates in 8-26 GHz frequency range fabricated in the normal single-layer Rogers RT/Duroid 5880 (tm) PCB process, offering the benefits of easy fabrication, large BW (both ABW and FBW), and acceptable IL. In addition, the comparison of the previously published results on coaxial line to SIW transitions with the results of the present work is also given in Table I. It is clearly shown that the proposed transition provides a very low transition area and is the most compact. The present work also achieved a low insertion loss and wider bandwidth than the reported works reflected in Table I. In contrast, the insertion loss is slightly more than [9], [18], and the overall loss is slightly higher than the reported in [7]–[12], [15], [18], [20], [21], [24]. It is noted that the insertion loss increases with the increase in frequency. For this cause, the authors restricted the comparison of insertion loss with reported in the higher frequency range. However, the overall loss is somewhat more due to the copper paste parameters spread and manual filling of the vias.

The figure of merit (FOM) defined as:

$$FOM = \frac{FBW(\%)}{(\frac{A}{\lambda_g^2})(IL)} \tag{3}$$

and evaluated for various transitions is also presented in Table I. Here FBW is the fractional bandwidth calculated at mid-band frequency, $\frac{A}{\lambda_g^2}$ is the normalized transition area (λ_g is the guided wavelength at midband frequency), and IL is the insertion loss (linear scale). Despite their lower FBW, SIW transitions [7], [8], [10]–[12], [18], [20], [22] are characterized by a relatively low FOM value. Other transitions [9], [18] have a lower FOM value due to a lower FBW, even their lower insertion loss and a better return loss. The presented work demonstrates high FOM because of low insertion loss, better return loss, wider FBW, and miniature size. For the transitions [9], [15], [21], [23], [24], the FOM cannot be calculated due to the insufficient data.

IV. Conclusion

In this paper, a new broadband coaxial line to SIW transition (in three versions) is proposed, analyzed, and implemented in the laboratory. The working frequency of these transitions is 8-26 GHz. The results for these transitions show improved performance compared to the known results. The proposed transitions have provided wider bandwidth, lower insertion loss, lower overall loss, reduction of the transition area, and low design complexity. The measured return loss, insertion loss, and overall loss are well-matched with the simulated ones.

References

[1] D. M. Pozar, *Microwave Engineering, 3rd ed*. New York: Wiley, 2005.

[2] A. Weisshaar, M. Mongiardo, and V. Tripathi, "Cad-oriented equivalent circuit modeling of step discontinuities in rectangular waveguides," *IEEE Microwave and Guided Wave Letters*, vol. 6, no. 4, pp. 171–173, 1996.

[3] R. Sorrentino, "Planar circuits, waveguide models, and segmentation method," *IEEE Transactions on Microwave Theory and Techniques*, vol. 33, no. 10, pp. 1057–1066, 1985.

[4] A. Tugulea and I. R. Ciric, "Two-dimensional equations for microwave planar circuits," in *1998 Symposium on Antenna Technology and Applied Electromagnetics*, 1998, pp. 315–318.

[5] D. Deslandes and K. Wu, "Integrated microstrip and rectangular waveguide in planar form," *IEEE Microwave and Wireless Components Letters*, vol. 11, no. 2, pp. 68–70, 2001.

[6] Z. Kordiboroujeni and J. Bornemann, "New wideband transition from microstrip line to substrate integrated waveguide," *IEEE Transactions on Microwave Theory and Techniques*, vol. 62, no. 12, pp. 2983–2989, 2014.

[7] T. Kai, Y. Katou, J. Hirokawa, M. Ando, H. Nakano, and Y. Hirachi, "A coaxial line to post-wall waveguide transition for a cost-effective transformer between a rf-device and a planar slot-array antenna in 60-ghz band," *IEICE Trans. Commun*, vol. E89-B, no. 5, pp. 1646–1654, 2006.

[8] Y. Uemichi, R. Hosono, N.Guan, J. Hirokawa, and M. Ando, "A simple through-hole based transformer between microstrip line and post-wall waveguide for millimeter-wave applications," *IEICE Trans. Electron*, vol. E97-C, no. 10, pp. 941–947, 2014.

[9] T. Kai, J. Hirokawa, M. Ando, H. Nakano, and Y. Hirachi, "A cost-effective transition between a microstrip line and a post-wall waveguide using a laminated ltcc substrate in 60-ghz band," *IEICE Trans. Commun*, vol. E90-C, no. 4, pp. 907–911, 2007.

[10] S. Mukherjee, P. Chongder, K. V. Srivastava, and A. Biswas, "Design of a broadband coaxial to substrate integrated waveguide (siw) transition," in *2013 Asia-Pacific Microwave Conference Proceedings (APMC)*, 2013, pp. 896–898.

[11] A. A. Khan and M. K. Mandal, "A compact broadband direct coaxial line to siw transition," *IEEE Microwave and Wireless Components Letters*, vol. 26, no. 11, pp. 894–896, 2016.

[12] A. A. Khan, M. Kahar, and M. K. Mandal, "A modified microstrip to empty substrate integrated waveguide transition," *International Journal of RF and Microwave Computer-Aided Engineering*, vol. 32, no. 2, p. e22990, 2022.

[13] L. Martinez, V. Laur, A. L. Borja, P. Queffelec, and A. Belenguer, "Low loss ferrite y-junction circulator based on empty substrate integrated coaxial line at ku-band," *IEEE Access*, vol. 7, pp. 104 789–104 796, 2019.

[14] S. Yang, Z. Yu, and J. Zhou, "A low-loss broadband planar transition from ground coplanar waveguide to substrate-integrated coaxial line," *IEEE Microwave and Wireless Components Letters*, vol. 31, no. 11, pp. 1191–1194, 2021.

[15] A. K. Nayak, I. M. Filanovsky, K. Moez, and A. Patnaik, "Broadband conductor backed-cpw with substrate-integrated coaxial line to siw transition for c-band," *IEEE Transactions on Circuits and Systems II: Express Briefs*, vol. 69, no. 5, pp. 2488–2492, 2022.

[16] U. Jankovic, A. Basu, and D. Budimir, "Planar transitions from substrate integrated coaxial line to single-layer transmission lines and waveguides," in *2018 IEEE MTT-S International Microwave and RF Conference (IMaRC)*, 2018, pp. 1–4.

[17] A. A. Khan, M. K. Mandal, and R. Shaw, "A compact and wideband sma connector to empty substrate integrated waveguide (esiw) transition," in *2015 IEEE MTT-S International Microwave and RF Conference (IMaRC)*, 2015, pp. 246–248.

[18] K. Zhu, Y. Xiao, W. Tan, H. Luo, and H. Sun, "A broadband e-band single-layer-siw-to-waveguide transition for automotive radar," *IEEE Microwave and Wireless Components Letters*, vol. 32, no. 6, pp. 523–526, 2022.

[19] A. K. Nayak, I. M. Filanovsky, K. Moez, and A. Patnaik, "A broadband coaxial line-to-siw transition using aperture-coupling method," *IEEE Microwave and Wireless Components Letters*, pp. 1–4, 2022.

[20] A. Morini, M. Farina, C. Cellini, T. Rozzi, and G. Venanzoni, "Design of low-cost non-radiative sma-siw launchers," in *2006 European Microwave Conference*, 2006, pp. 526–529.

[21] Z. Liu, J. Xu, and W. Wang, "Wideband transition from microstrip line-to- empty substrate-integrated waveguide without sharp dielectric taper," *IEEE Microwave and Wireless Components Letters*, vol. 29, no. 1, pp. 20–22, 2019.

[22] S. Choudhury, A. Mohan, and M. Bozzi, "A coaxial to air-filled substrate integrated waveguide transition with near-octave bandwidth," *IEEE Microwave and Wireless Components Letters*, vol. 32, no. 11, pp. 1275–1278, 2022.

[23] A. Belenguer, H. Esteban, and V. E. Boria, "Novel empty substrate integrated waveguide for high-performance microwave integrated circuits," *IEEE Transactions on Microwave Theory and Techniques*, vol. 62, no. 4, pp. 832–839, 2014.

[24] E. Arnieri, F. Greco, L. Boccia, and G. Amendola, "Vertical waveguide-to-microstrip self-diplexing transition for dual-band applications," *IEEE Microwave and Wireless Components Letters*, vol. 32, no. 12, pp. 1407–1410, 2022.

[25] B. Thomas, "Design of corrugated conical horns," *IEEE Transactions on Antennas and Propagation*, vol. 26, no. 2, pp. 367–372, 1978.

[26] J. Qi, Y. Dang, P. Zhang, H. Chou, and H. Ju, "Dual-band circular-polarization horn antenna with completely inhomogeneous corrugations," *IEEE Antennas and Wireless Propagation Letters*, vol. 19, no. 5, pp. 751–755, 2020.

[27] L. Periasamy and A. J. Gasiewski, "Antenna design and prelaunch performance of a low-cost 118.75 ghz temperature sounding cubesat radiometer with 3-d-printed corrugated feed and offset reflector optics," *IEEE Transactions on Antennas and Propagation*, vol. 68, no. 6, pp. 4881–4893, 2020.

[28] K. W. Eccleston, "Half-mode buried corrugated substrate integrated waveguide," *IEEE Microwave and Wireless Components Letters*, vol. 24, no. 4, pp. 215–217, 2014.

[29] K. Chen, Y. H. Zhang, S. Y. He, H. T. Chen, and G. Q. Zhu, "An electronically controlled leaky-wave antenna based on corrugated siw structure with fixed-frequency beam scanning," *IEEE Antennas and Wireless Propagation Letters*, vol. 18, no. 3, pp. 551–555, 2019.

[30] T. Lou, X. Yang, H. Qiu, Q. Luo, and S. Gao, "Low-cost electrical beam-scanning leaky-wave antenna based on bent corrugated substrate integrated waveguide," *IEEE Antennas and Wireless Propagation Letters*, vol. 18, no. 2, pp. 353–357, 2019.

[31] Y. Lin, Y. Zhang, H. Liu, Y. Zhang, E. Forsberg, and S. He, "A simple high-gain millimeter-wave leaky-wave slot antenna based on a bent corrugated siw," *IEEE Access*, vol. 8, pp. 91 999–92 006, 2020.

[32] Y. Zhang, H. Liu, C. Meng, Y. Lin, Y. Zhang, E. Forsberg, and S. He, "A broadband high-gain circularly polarized wide beam scanning leaky-wave antenna," *IEEE Access*, pp. 1–1, 2020.

[33] D. Deslandes, "Design equations for tapered microstrip-to-substrate integrated waveguide transitions," in *2010 IEEE MTT-S International Microwave Symposium*, 2010, pp. 704–707.

[34] A. K. Nayak and A. Patnaik, "Design of an siw corrugated h-plane horn antenna with improved performance," in *2017 IEEE Applied Electromagnetics Conference (AEMC)*, 2017, pp. 1–2.

[35] A. K. Nayak, V. Singh Yadav, and A. Patnaik, "Wideband transition from tapered microstrip to corrugated siw," in *2019 IEEE MTT-S International Microwave and RF Conference (IMARC)*, 2019, pp. 1–4.

[36] W. Hong, B. Liu, Y. Wang, Q. Lai, H. Tang, X. X. Yin, Y. D. Dong, Y. Zhang, and K. Wu, "Half mode substrate integrated waveguide: A new guided wave structure for microwave and millimeter wave application," in *2006 Joint 31st International Conference on Infrared Millimeter Waves and 14th International Conference on Teraherz Electronics*, 2006, pp. 219–219.

Anil Kumar Nayak (S'14 and M'24) received the B.Tech. Degree in Electronics and Telecommunication Engineering from the Biju Patnaik University of Technology (BPUT), Rourkela, India, in 2007, the M.Tech. Degree in RF and Microwave Engineering from IIT Kharagpur, Kharagpur, India, in 2016 and Ph.D. in RF and Microwave Engineering from IIT Roorkee, Roorkee, India, in June 2023. Currently, he is working as a Postdoctoral Fellow in Dept. of Electrical Engineering at IIT Indore; his current research interests include substrate-integrated waveguide (SIW) transitions, composite right-left hand (CRLH) material for future communication, frequency reconfigurable, ultrawide-band, and computational electromagnetic, In-band and out-band full duplex antenna, Implantable antenna for biomedical application, and on-chip antennas. He is a Senior International Union of Radio Science (URSI) International and IEEE Member. SERB awarded him the Overseas Visiting Doctoral Fellowship, Government of India, to conduct part of his research work at the University of Alberta, Edmonton, AB, Canada, in 2021(18 months). He has received six best paper awards and seventeen travel grants from different international conferences of international repute. He also received a prestigious IEEE APS student travel grant in 2022. He served as the secretary for the IEEE MTTS-S Student Branch Chapter, IIT Roorkee, from October 2020 to the end of 2022. He also serves as a Regular Reviewer for journals such as IEEE MWTL, IEEE TCAS II, IEEE AWPL, IET MAP, MOTL, IEEE ACCESS, IEEE TRANSACTIONS ON CONSUMER ELECTRONICS and IEEE TRANSACTIONS ON COMPUTER-AIDED DESIGN OF INTEGRATED CIRCUITS AND SYSTEMS. He has published 52 internationally reputed patents, IEEE transactions, journals, letters, book chapters, and conferences.

Igor M. Filanovsky (Life Senior Member, IEEE) is currently a Professor Emeritus with the Department of Electrical Engineering, University of Alberta, Edmonton, AB, Canada. His current research interests include network analysis and synthesis, oscillations theory and applications, and analog microelectronics. He has published more than 200 articles on these topics in IEEE journals and conference proceedings.

Dr. Filanovsky has served two terms as an Associated Editor for IEEE TRANSACTIONS ON CIRCUITS AND SYSTEMS-I: REGULAR PAPERS. He is currently an Associate Editor of the *International Journal of Circuit Theory and Applications.*

Kambiz Moez (Senior Member, IEEE) received the B.Sc. degree in electrical engineering from the University of Tehran, Tehran, Iran, in 1999, and the M.Sc. and Ph.D. degrees from the University of Waterloo, Waterloo, ON, Canada, in 2002 and 2006, respectively. Since January 2007, he has been with the Department of Electrical and Computer Engineering, University of Alberta, Edmonton, AB, Canada, where he is currently a Full Professor and the Associate Dean Undergraduate Students - ECE. His research interests include the analysis and design of analog, radio frequency, and millimeter-wave CMOS integrated circuits and systems for a variety of applications, including wired/wireless communications and sensors, radio frequency energy harvesting, biomedical imaging, instrumentations, radars, and power electronics. He has authored or co-authored over 100 peer-reviewed journal articles and conference papers in his field of research.

Dr. Moez is a Registered Professional Engineer in the province of Alberta. He is currently serving as an Associate Editor for IET Electronics Letter.

Amalendu Patnaik received the Ph.D. degree in electronics from Berhampur University, Berhampur, India, in 2003. From 2004 to 2005, he was with The University of New Mexico, Albuquerque, NM, USA, as a Visiting Scientist. He is currently a Professor with the Department of Electronics and Communication Engineering, Indian Institute of Technology Roorkee, Roorkee, India. He has authored/coauthored more than 150 peer-reviewed papers in international journals and conferences, and coauthored 1 book on Compact Antennas for High Data Rate Communication: Ultra-Wideband (UWB) and Multiple-Input Multiple-Output (MIMO) Technology (Springer) and 1 book chapter on Neural Networks for Antennas in Modern Antenna Handbook (Wiley). His current research interests include plasmonic antennas, antenna array signal processing, applications of soft-computing techniques in electromagnetics, CAD for patch antennas, EMI, and EMC. Dr. Patnaik is a recipient of the IETE Sir J. C. Bose Award in 2000, the URSI Young Scientist Award in 2005, and the BOYSCAST Fellowship from the Department of Science and Technology, Government of India, from 2004 to 2005. He was the Chairperson of the IEEE Roorkee Subsection from 2015 to 2017. He is currently the Chair of the IEEE Uttar Pradesh section AP-S Chapter. He was an IEEE AP-S Region-10 Distinguished Speaker during 2015-2016. He is an Editorial Board Member of the International Journal of RF and Microwave Computer-Aided Engineering (Wiley).